The Astronomical Journal, 126:1415–1422, 2003 September

THE LACK OF BLUE SUPERGIANTS IN NGC 7419, A RED SUPERGIANT–RICH GALACTIC OPEN CLUSTER WITH RAPIDLY ROTATING STARS

Geneviève Caron, Anthony F. J. Moffat, Nicole St-Louis, and Gregg A. Wade[1]
Département de Physique, Université de Montréal, C.P. 6128, Succursale Centre-Ville, Montréal, QC H3C 3J7, Canada;
and Observatoire du Mont Mégantic; genpat@videotron.ca, moffat@astro.umontreal.ca,
stlouis@astro.umontreal.ca, Gregg.Wade@rmc.ca

and

John B. Lester
Department of Astronomy, University of Toronto at Mississauga, 3359 Mississauga Road North,
Mississauga, ON L5L 1C6, Canada; lester@astro.utoronto.ca
Received 2003 January 15; accepted 2003 May 28

ABSTRACT

According to previous studies based on photometry alone, NGC 7419 reveals a surprisingly low ratio of blue to red supergiants: only one blue supergiant (BSG) along with a record number of five red supergiants (RSGs). However, for a cluster like NGC 7419 with solar metallicity, one expects twice as many BSGs as RSGs. To verify the small ratio of BSGs to RSGs, we have obtained spectroscopic observations of the seven most luminous blue member stars using the 1.6 m telescope of the Mount Mégantic Observatory. (The RSGs have already been studied spectroscopically.) To classify the stars, we have developed a system especially adapted for these heavily reddened stars in a spectral region from 8400 to 8920 Å, near the hydrogen Paschen series limit. This classification system is based on standard stars of known MK spectral type extending over O9–B5 and all luminosity classes and is linked through a grid of synthetic spectra to the atmospheric physical parameters $T_{\rm eff}$ and $\log g$. We also include Be stars. Among the seven blue stars observed in NGC 7419, four have red spectra that are dominated by absorption lines and three by emission lines. The spectral types for the former are B2.5 II–III, B2.5 III, B0 III, and B4 III (e), while those for the latter are Be, B1 III–Ve, and Be, respectively. The average heliocentric radial velocity of these stars is -66 ± 6 km s^{-1}, compatible with the value of -74 ± 9 km s^{-1} measured for the five RSG members. A distance of 1.7 ± 0.4 kpc for this cluster was estimated using the blue-star spectral types, in agreement with the value of 2.3 ± 0.3 kpc found by Beauchamp and coworkers, based on isochrone fitting in the color-magnitude diagram. With no BSG stars detected spectroscopically, we confirm the low number, in this case absence, of BSGs in this cluster. The high fraction of Be stars detected by us and others among the bright blue member stars could be explained by an average rotational velocity for the stars in NGC 7419, which is significantly higher than in other clusters of similar age and metallicity. Since higher stellar rotation rates shorten the BSG phase, we suggest that this explains why the evolved stars in NGC 7419 have become RSGs. Thus, NGC 7419 is an exceptional case, since high stellar rotation normally tends to occur at lower metallicity.

Key words: open clusters and associations: individual (NGC 7419) — stars: emission-line, Be — stars: rotation — supergiants

1. THE PROBLEM OF THE BLUE-TO-RED SUPERGIANT RATIO IN OPEN STAR CLUSTERS

The blue-to-red supergiant ratio as a function of metallicity is important to constrain the nature of supernova progenitors in different environments (Langer 1991a, 1991b; Tuchman & Wheeler 1989a, 1989b) and the evolution of massive stars in regions of intense star formation (Cervino & Mas-Hesse 1994; Origlia et al. 1999). The blue-to-red ratio is an important characteristic of the population of massive stars in stellar clusters and galaxies (Langer & Maeder 1995) because supergiants can be seen out to great distances in the universe.

Observations show that the blue-to-red ratio increases rapidly with metallicity (Maeder & Meynet 2000; Cowley et al. 1979; Humphreys & McElroy 1984; Schulte-Ladbeck & Hopp 2001). Present-day evolutionary models including rotation (Maeder & Meynet 2001) *are* able to reproduce this effect.

NGC 7419, shown in Figure 1, is a young open cluster near the Galactic plane in the constellation of Cepheus ($l = 109\overset{\circ}{.}14$, $b = +1\overset{\circ}{.}14$). It has a tidal radius of $\sim 5'$ (3.4 pc at a distance of 2.3 ± 0.3 kpc) with an age of 14 ± 2 Myr. These values have been obtained by Beauchamp, Moffat, & Drissen (1994) using the isochrones of Maeder & Meynet (1989). The mass function between 1.5 and 10 $M_\odot$ follows that of Salpeter, $N(M) \sim M^\gamma$, with $\gamma = 2.25 \pm 0.10$.

This cluster is particularly interesting because the photometric study by Beauchamp et al. (1994) shows that it contains a record number of five red supergiants (RSGs) but, at most, only one possible blue supergiant (BSG), star 687. This is the brightest blue cluster member, being denoted as a bright giant based on its position in a color-magnitude diagram (CMD). (Our current study yields B2.5 II–III for this star, putting it just below the limit to be labeled as a BSG.) The resulting blue-to-red supergiant ratio of 0.2 ± 0.2 is considerably lower than the ratio of 1.9 ± 0.8 found for 11 other clusters of the same age and Galactocentric distance. Therefore, NGC 7419 seems to be behaving like a low-metallicity cluster.

[1] Current address: Department of Physics, Royal Military College of Canada, P.O. Box 17000, Station Forces, Kingston, ON K7K 4B4, Canada.

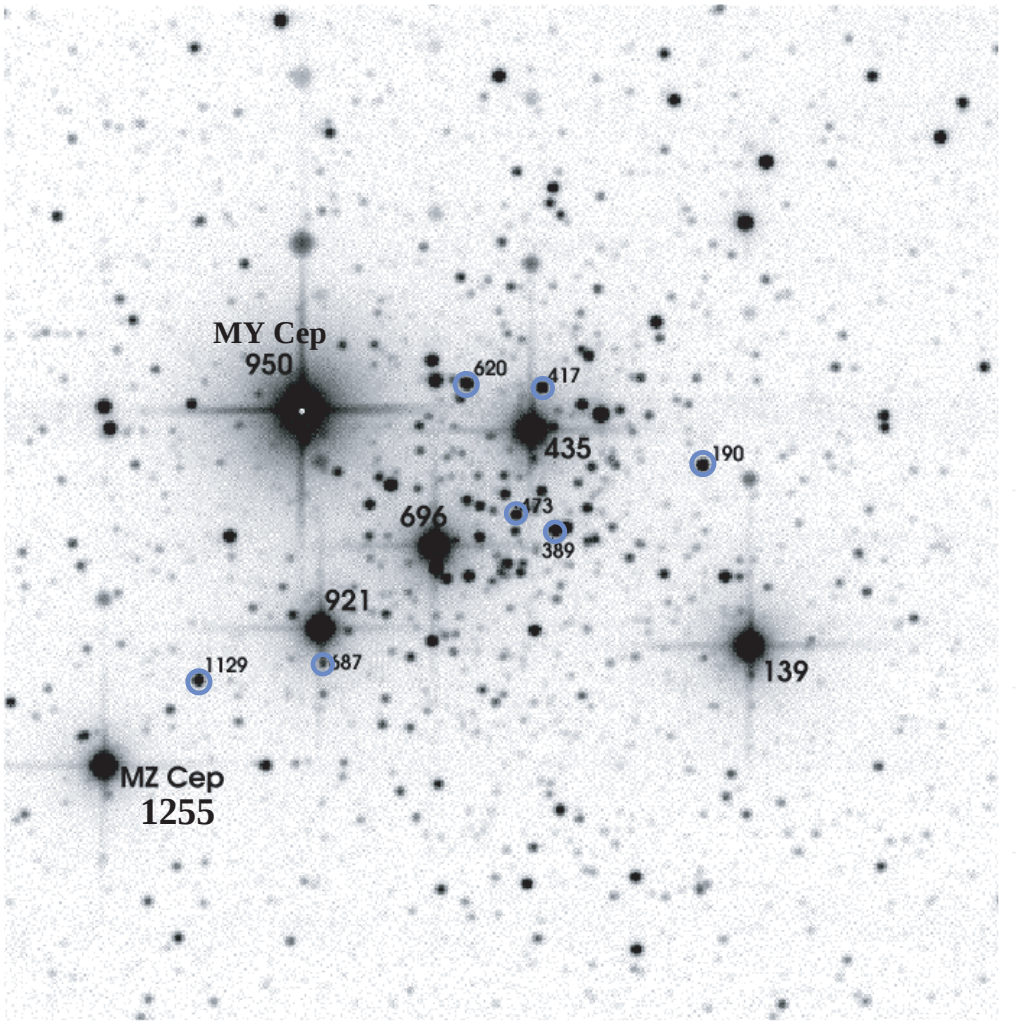

FIG. 1.—The *K*-band identification chart of NGC 7419 taken from the 2MASS survey. The five RSGs (and the nearby field carbon star MZ Cep) are indicated by large numbers while the seven observed brightest blue cluster members are indicated by small numbers and circled in blue. The numbers are from Beauchamp et al. (1994).

The color-magnitude diagram of Beauchamp et al. (1994) is shown in Figures 2 and 3. The photometry suggests that there are few if any BSG stars in NGC 7419. However, since the evolutionary tracks used are not sufficiently accurate in the blue region of the diagram, it is impossible to distinguish with certainty if the bright blue stars are on the main sequence or if they are in the supergiant phase. Cluster membership is judged solely on the basis of position in the CMD.

In order to verify these results for NGC 7419, we have used the more accurate spectroscopic technique as opposed to photometry alone. Since NGC 7419 is highly extincted ($A_v = 6.7$) and its brightest blue stars are optically faint ($B \sim 15$–16), we have devised a spectroscopic classification system in the red wavelength range and applied it to the seven bluest stars in NGC 7419.

2. OBSERVATIONS

In order to establish a classification system in the red, a total of 55 standard absorption-line and 15 emission-line stellar spectra were observed between 1999 November and 2001 January using the Cassegrain long-slit spectrograph and 2048 × 2048 Loral CCD at the 1.6 m telescope of the Observatoire du mont Mégantic (Québec). The wavelength coverage spans 8200–9200 Å with an inverse dispersion of 0.48 Å pixel^{-1}. Because of the high density of telluric lines, the usable wavelength coverage spans only between 8400 and 8920 Å. For the seven brightest blue member stars in NGC 7419, a combination of seven exposures of 50 minutes each yielded a typical signal-to-noise ratio of ~100. The net signal-to-noise ratio for the standard stars was typically 200–700. The standards span O9–B5 and V–Ia and include Be stars. The data reduction was performed in the usual manner using the standard IRAF software packages supported by the IRAF programing group at NOAO in Tucson, Arizona.

3. A NEW STELLAR CLASSIFICATION SYSTEM FOR LATE-O TO MID-B STARS IN THE RED

In Figures 4 and 5, we present montages of samples of standard stars with approximately the same luminosity class in each but of varying spectral type. The dominant lines are

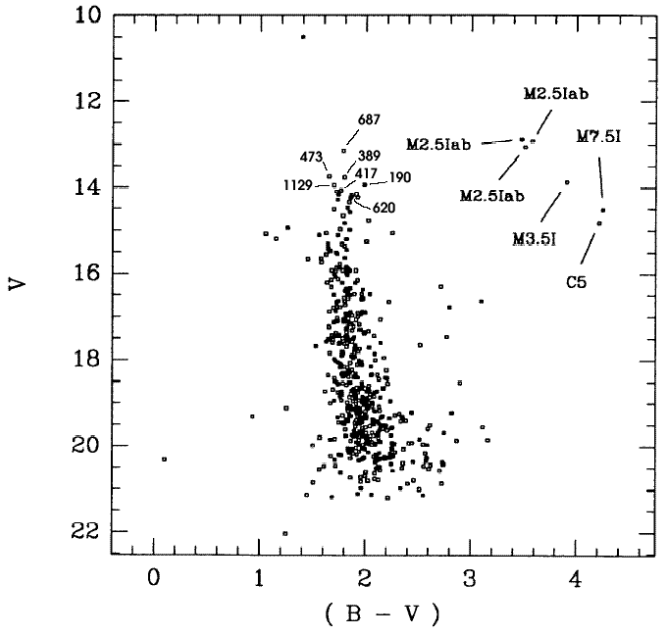

FIG. 2.—Color-magnitude diagram of NGC 7419 from Beauchamp et al. (1994) showing the five known RSGs (plus the field carbon star) along with the seven identified brightest blue member stars. The brightest star at the top of the figure is a field star.

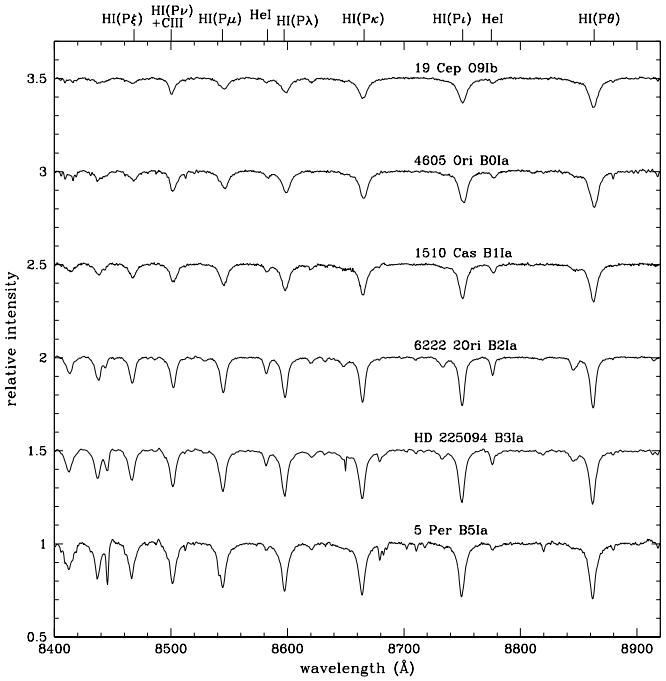

FIG. 4.—Montage of standard supergiant spectra ranging from O9 to B5.

the neutral hydrogen lines of the Paschen series and some neutral helium lines. From these plots, we see that the lines for dwarfs are always broader than the corresponding lines for supergiants, as expected as a consequence of the increasing surface gravity. Furthermore, the equivalent widths of most lines increase with advancing spectral type. We can thus expect that the measurement of the equivalent widths and FWHMs of the spectral lines will serve well to distinguish the various spectral types and luminosity classes.

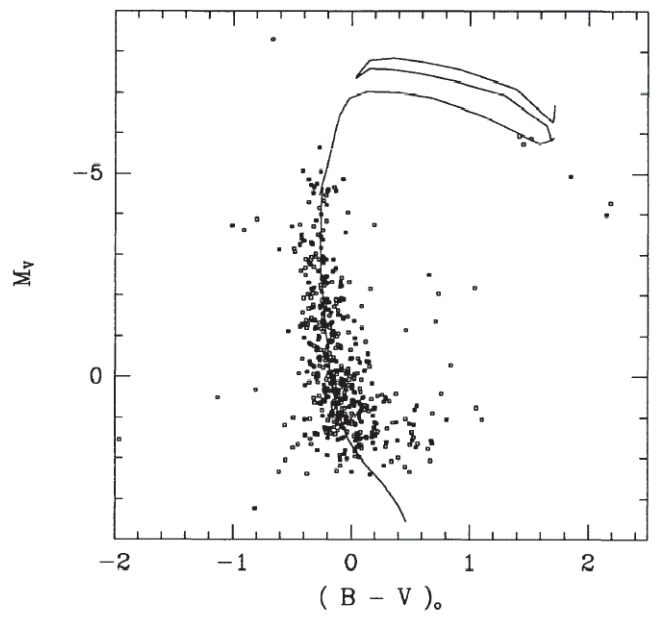

FIG. 3.—Color-magnitude diagram of NGC 7419 from Beauchamp et al. (1994) corrected for global extinction and superposed on an isochrone for an age of $10^{7.2}$ yr.

We note that hydrogen lines are not commonly employed to classify B stars. However, there is no other option in the present case. For example the O I λ8446 line might have been a good candidate, but it is too weak to be useful here.

Figure 6 shows the FWHM of the Paκ line of H I (λ8664) as a function of the FWHM of the He I λ8777 line for each standard star. In this plot, we have delimited the approximate zones for the different luminosity classes. We see that

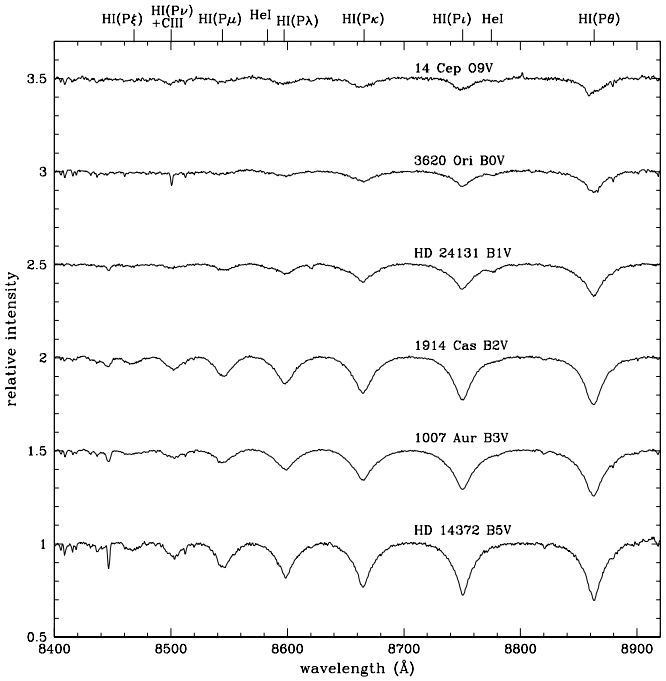

FIG. 5.—Montage of standard main-sequence spectra ranging from O9 to B5.

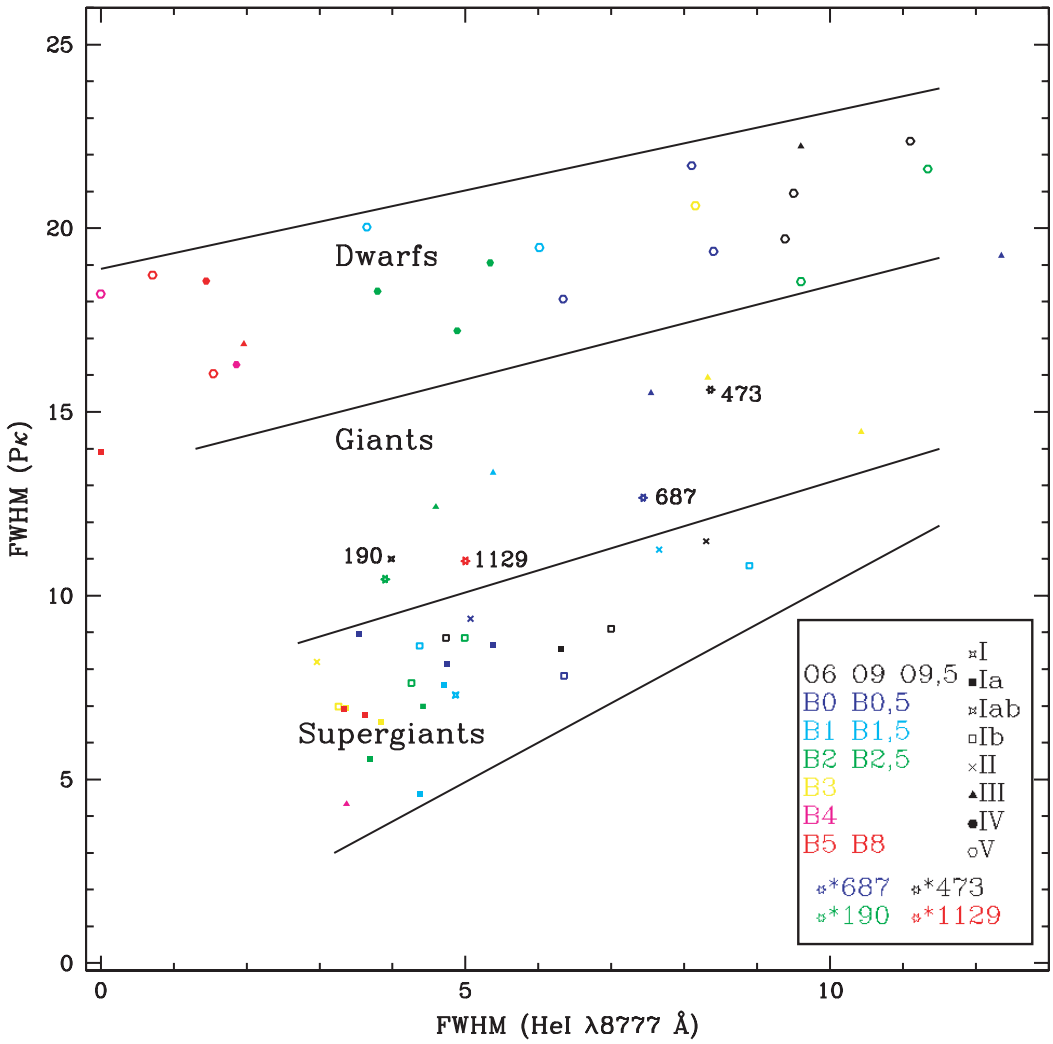

FIG. 6.—FWHM of Paκ vs. the FWHM of He I (λ8777). The color code is indicated.

the four absorption-line member stars of NGC 7419 lie near the border between giants and supergiants. To determine more accurately the spectral types and luminosity classes of these stars, we have plotted the equivalent widths of all Paschen lines of H I (Paι, Paκ, Paλ, Paμ, Paν + C III, and Paξ) for the standard stars as well as the NGC 7419 stars as a function of the equivalent width of Paθ (Fig. 7). We have added curves of approximately constant spectral type and luminosity class on each graph to facilitate interpolation.

The dominant physical effects that modify the equivalent width of the Paschen lines are temperature and pressure in the line-forming region. When the temperature increases, the number of ionized atoms increases according to the Saha equation, which for the hot stars implies a decrease of the equivalent width of the hydrogen lines of the Paschen series.[2] The pressure (or gravity) produces a higher range of equivalent widths for the dwarfs than for the supergiants. This is the result of the Stark effect, which increases the equivalent width of the lines of the dwarfs relative to that of the giants/supergiants as a consequence of increased line wing absorption.

Aller (1963) has shown that the atomic line absorption coefficient (α), on which the shape of a spectral line depends, is, when applied to the line wings, a linear function of the electron pressure (P_e) and an interaction constant (C_u). The asymptotic behavior of the line absorption coefficient in the hydrogen line wing (Gray 1992, eq. [11.43]) is

$$\alpha(\Delta\lambda)\ [\mathrm{cm}^2\ \text{per absorber}] = 321 C_u \frac{P_e}{T} \Delta\lambda^{-5/2}\ , \qquad (1)$$

with $\Delta\lambda$ the wavelength separation from line center in units of angstroms, P_e in dyne per square centimeter, and T in kelvins. While this equation applies to the Balmer series, the form should also be applicable to the Paschen series. The key point is that the coefficient C_u decreases for higher members of the series. Hence, for instance, the broadening caused by the Stark effect is larger for the Paθ line than for the Paμ line.

As the gravity increases the electron gas pressure increases, leading to a greater Stark effect and hence wing absorption. Since the relative effect is the same for all Paschen lines, we expect that each line will increase in breadth and equivalent width at the same rate. However, as

[2] This is for LTE. However, the lines of B stars become increasingly affected by departures from LTE, going from B9 to B0, i.e., are more ionized than the T_{eff} would predict because of the increasing importance of radiation over collisions.

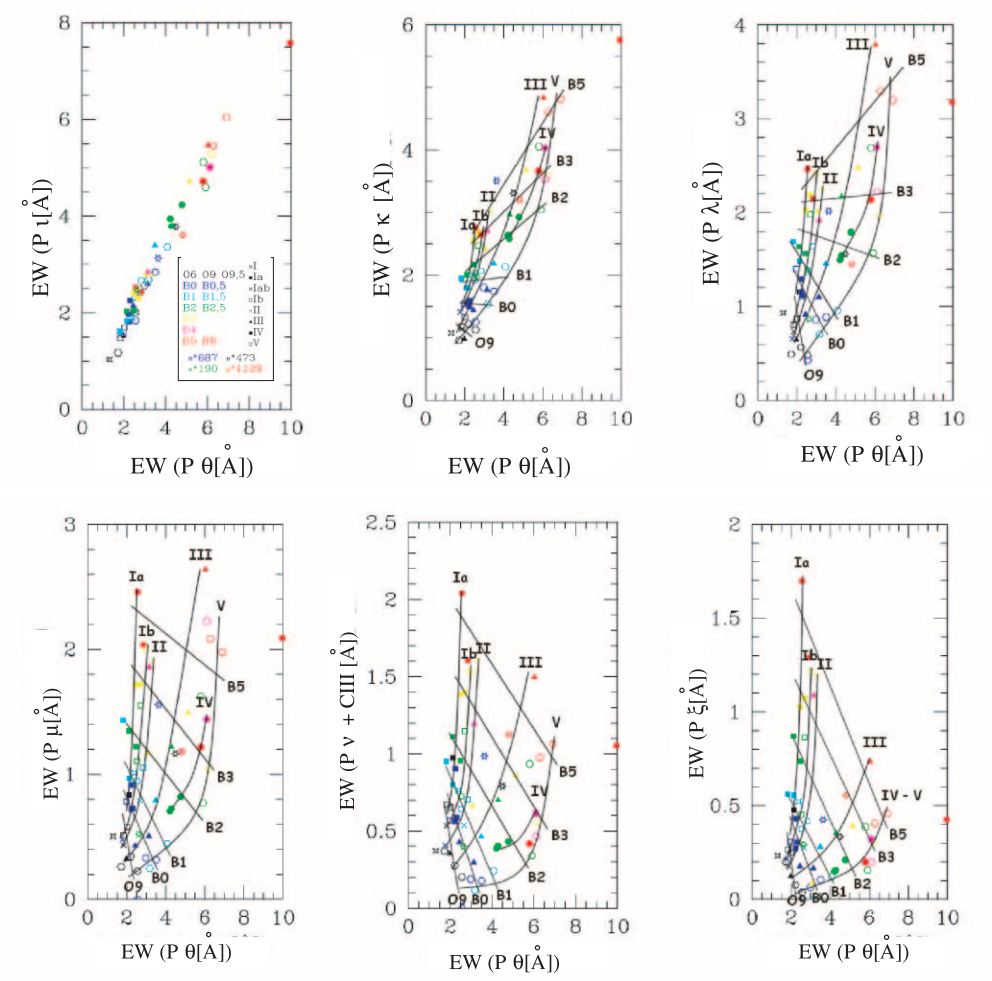

FIG. 7.—Behavior of the equivalent width of various Paschen lines vs. the equivalent width of Paθ for our standard absorption-line stars. Paθ was chosen as a reference because it is the lowest series member observed. The positions of the four absorption-line cluster stars are also indicated.

the pressure increases, we initially observe a stronger effect for the higher Paschen members, then tapering off at very high pressure. This is caused by the fact that the lines become increasingly blended toward the upper limit of the Paschen series. Since the pressure at the surface of dwarf stars is higher than for supergiants, the blending is greater. This explains why we observe an increased reduction of equivalent width for the higher line members when going from supergiant to dwarf stars.

Note that we normalize the observed spectra to a pseudocontinuum resulting from the blended wings of Paschen lines near the series limit. Therefore, the measured EW-$T_{\rm eff}$-log g relationship is not necessarily intuitive, as we are always measuring EW contributions from several lines simultaneously. Thus, to provide a theoretical basis for our empirical classification system, we calculated spectral models at solar metallicity using ATLAS9 (Kurucz 1993) with the SYNTHE code at the University of Toronto. The models' sample temperatures were between 15,000 and 35,000 K and gravities between log g (cm s^{-2}) = 2.5 and 4.75. The synthetic spectra were convolved with an instrumental Gaussian profile of FWHM = 4.0 pixels. To test whether rotation has an influence on the results, we convolved a synthetic spectrum with $v \sin i = 150$ km s^{-1}. The resulting EWs did not change by more then 0.2 Å for any line. Therefore, we simply used the nonrotation spectra. Then we measured the equivalent widths of the Paschen lines in the same way as for the observed spectra. We then superposed these values as a grid on our classification plots (see Fig. 8). The models and observations agree well: log g ranges from 2.5 to 3.0 for supergiants, from 3.5 to 4.25 for giants, and from 4.5 to 5.0 for dwarfs. The key point here is that the observed EW-$T_{\rm eff}$-log g relationship can be completely recovered by measuring synthetic spectra in exactly the same way (e.g., normalized to the pseudocontinuum and measured blended EWs). Figure 9 shows for clarity a synthetic spectrum not normalized to the pseudocontinuum.

4. APPLYING THE NEW SYSTEM TO NGC 7419

Figure 10 shows a montage of the observed spectra for the seven brightest member blue stars of NGC 7419 in order of decreasing visual luminosity. The identification numbers are from Beauchamp et al. (1994).

Note that four stars (687, 473, 190, and 1129) appear to have only absorption lines, while three stars (389, 417, and 620) have emission lines. Star 1129 shows a weak emission component, since the bottoms of its lines are slightly flattened. This agrees with the weak-line Be nature of this star assigned by Pigulski & Kopacki (2000). We then assigned spectral types and luminosity classes to the four absorption-line stars using our classification system. The emission-line

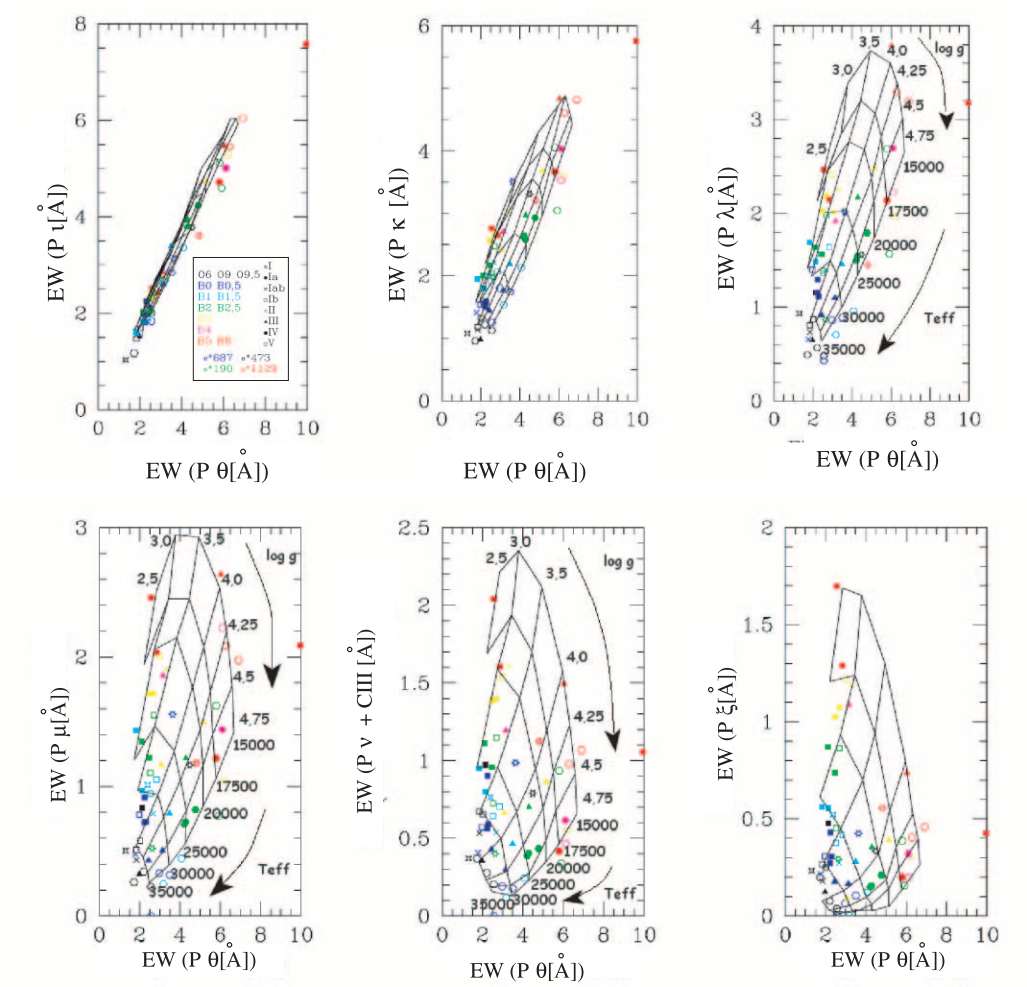

FIG. 8.—Behavior of the equivalent width of various Paschen lines vs. the equivalent width of Pθ for our standard absorption-line stars along with the synthetic grid.

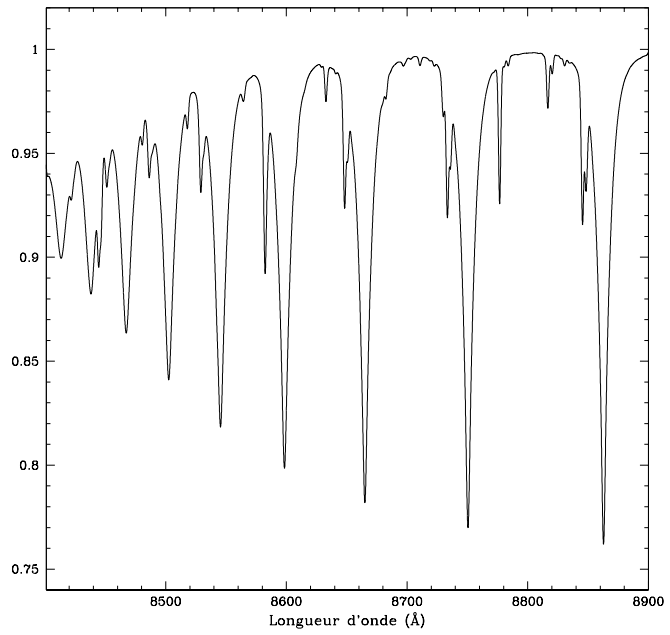

FIG. 9.—Example of a synthetic spectrum with $T_{\rm eff} = 20,000$ K and $\log g$ (cm s^{-2}) = 3.0, without normalizing to a pseudocontinuum.

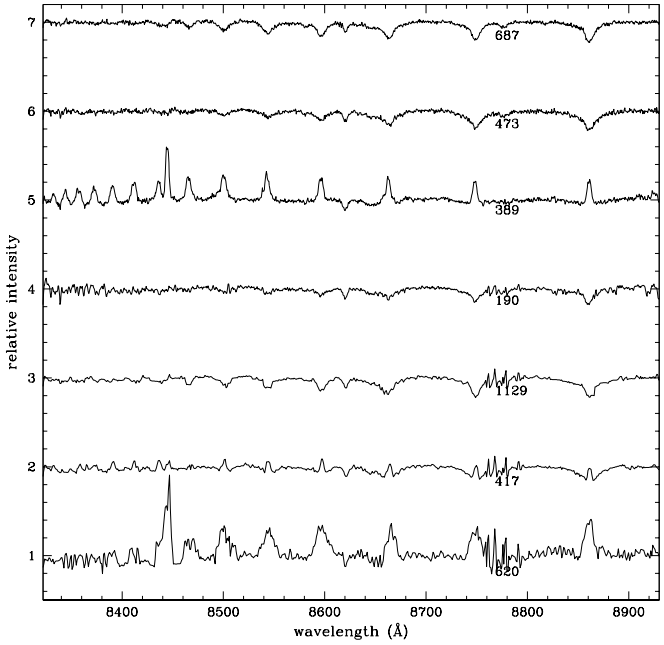

FIG. 10.—Observed spectra of the seven brightest blue member stars of NGC 7419, in order of decreasing visual brightness from top to bottom. The increased noise at 8750–8790 Å comes from incomplete sky subtraction, which is worse for fainter stellar magnitudes.

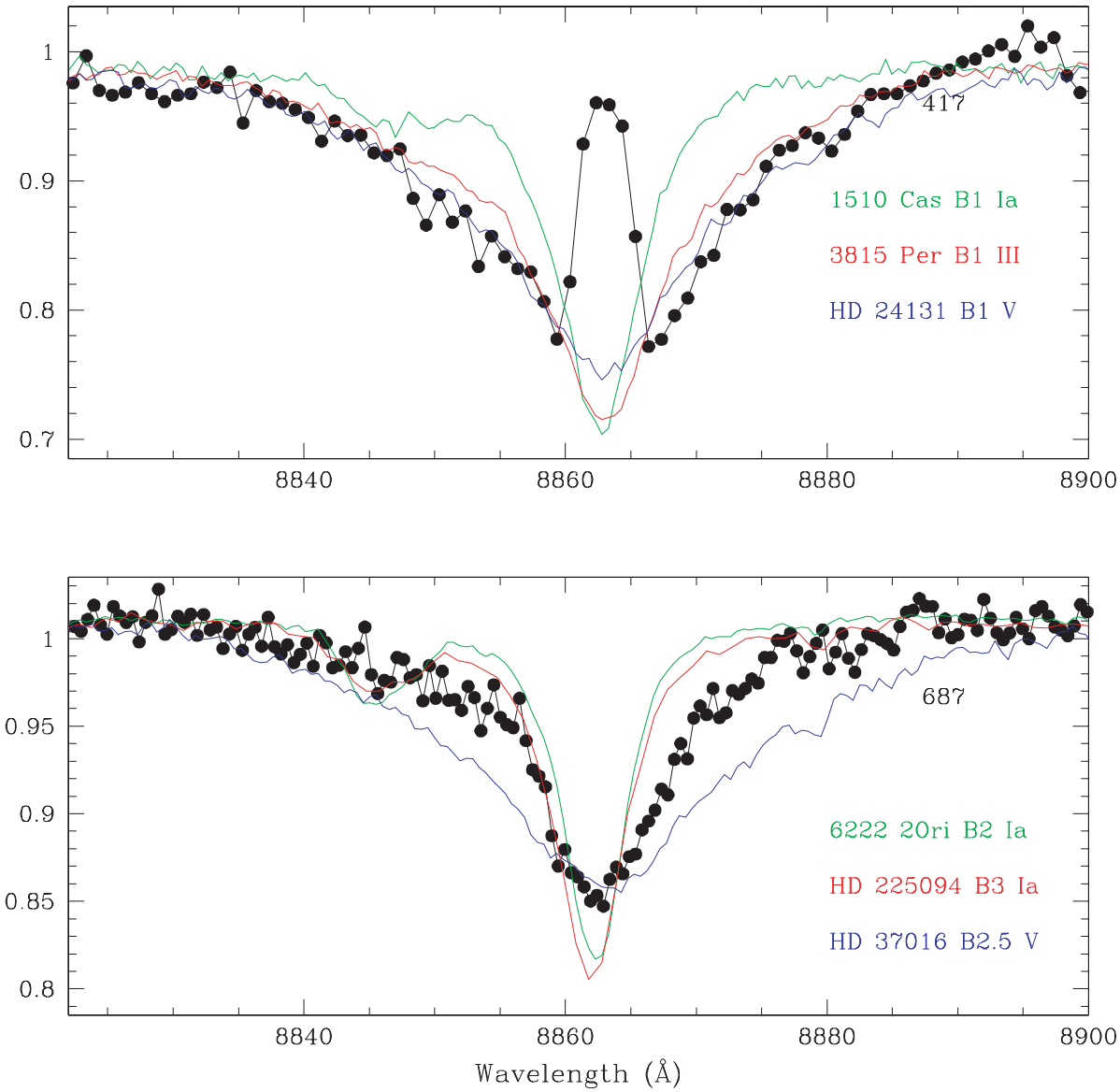

FIG. 11.—Comparison of the Pθ line in star 417 (*dots joined by lines*) with that of three standard non–emission-line stars of spectral type B1 in a range of luminosity classes. *Bottom*: Same for the star 687, the brightest member blue star in NGC 7419.

stars of NGC 7419 were visually compared with the emission-line standards. Stars 389 and 620 have a strong emission component, while star 417 displays weaker emission. Furthermore, since these stars do not exhibit P Cygni type profiles, we conclude that they are not BSGs. The wide diversity of spectra from the emission-line stars prevents us from making an exact classification for these stars. Nevertheless, it is likely that stars 389 and 620 are early Be stars, since they both show the characteristic Be-star O I line (λ8446) in emission. To classify star 417, we superposed several absorption-line standards on its spectrum. Figure 11 shows a comparison of the wings of the Paθ line. We find that star 417 shows the depth of a B1 star, while the wings show a luminosity class of III–V, and we adopt an approximate spectral classification of B1 III–Ve. This figure also shows that even the brightest blue member star in NGC 7419 is not a blue supergiant.

Table 1 summarizes the spectral types and luminosity classes that we determined from Figure 7 and the effective temperatures and gravities that we determined from Figure 8. *Since the seven brightest blue member stars of NGC 7419 are clearly not supergiants, we conclude that NGC 7419 contains no BSGs at all.* Beauchamp et al.'s (1994) claim of

TABLE 1
SUMMARY RESULTS FOR THE SEVEN BRIGHTEST BLUE MEMBER STARS IN NGC 7419

Stars	Spectral Type	$T_{\rm eff}$ (K)	log g
687	B2.5 II–III	23000 ± 2000	3.7 ± 0.2
473	B2.5 III	21000 ± 2000	4.1 ± 0.2
389	Be	...	...
190	B0 III	31000 ± 2000	4.1 ± 0.2
1129	B4 III(e)	19000 ± 2000	3.9 ± 0.2
417	B1 III–Ve	...	...
620	Be	...	...

one possible BSG was based on less sensitive photometric data and was a luminosity class II star, i.e., a bright giant, in any case.

5. WHY ARE THERE NO BLUE SUPERGIANTS IN NGC 7419?

Pigulski & Kopacki (2000) have also recently reported that NGC 7419 contains a relatively large number of Be stars. From CCD photometry in narrowband Hα and broadband Cousins filters R_C and I_C, they found 31 Be stars, leading to a lower limit for the $\mathrm{Be}/\mathrm{B}_{\mathrm{total}}$ ratio ($R_C < 16.1$) of $36\% \pm 7\%$.

For several young open clusters with reliable data and in the age range of 11–21 Myr (i.e., for a viable sample straddling the age of NGC 7419), we compare in Figure 12 the frequency of RSGs [RSG/(BSG + RSG)] with the frequency of Be stars [Be/(B + Be)]. The number of supergiants was taken from Mermilliod & Maeder (1986), while the frequency of Be stars is from Schild & Romanishin (1976). In this age range, the data do indicate significant numbers of all of these types at all ages. The error bars are based on Poisson statistics: $\sigma_{N_i}^2 = N_i$, where N_i is RSG, BSG, Be, or B and

$$\sigma_{\mathrm{RSG/tot}} = \sqrt{\frac{\mathrm{BSG} \times \mathrm{RSG}}{(\mathrm{BSG} + \mathrm{RSG})^3}}, \quad \sigma_{\mathrm{Be/tot}} = \sqrt{\frac{\mathrm{Be} \times \mathrm{B}}{(\mathrm{B} + \mathrm{Be})^3}}. \tag{2}$$

Of course the true errors may be somewhat larger due to systematic effects. However, we have no obvious way of quantifying such errors. For example, while Keller, Wood, & Bessell (1999) find no correlation of Be-star fraction with metallicity, Maeder, Grebel, & Mermilliod (1999) do find such a correlation, based on a larger sample. We prefer retaining as large a uniform sample as possible. Even though the Poisson-based error bars are large, Figure 12 seems to indicate a direct relationship between the relative frequencies of RSG and Be stars. When the relative number of red supergiants is small, the Be-star frequency is also small. Maeder (2003, private communication) has recently found a similar effect (based on a larger sample), reflected in an increase of both relative numbers of RSG and Be stars with decreasing metallicity.

Assuming that Be stars indicate rapid rotation, we suggest that the fraction of RSGs increases as the rotation increases. Maeder & Meynet (2000, 2001) have found that rotation is a very important factor for stellar evolution in clusters. These authors also find that fast rotation tends to occur at low metallicity, due to weaker winds leading to reduced loss of angular momentum. Rapid rotation transports helium to the hydrogen shell burning zone, rendering the burning less efficient and the associated convective zone smaller. The stellar radius can then expand in the helium-burning phase and lead to an RSG star. This leads to a higher rate of RSG and Be star formation at low metallicity.

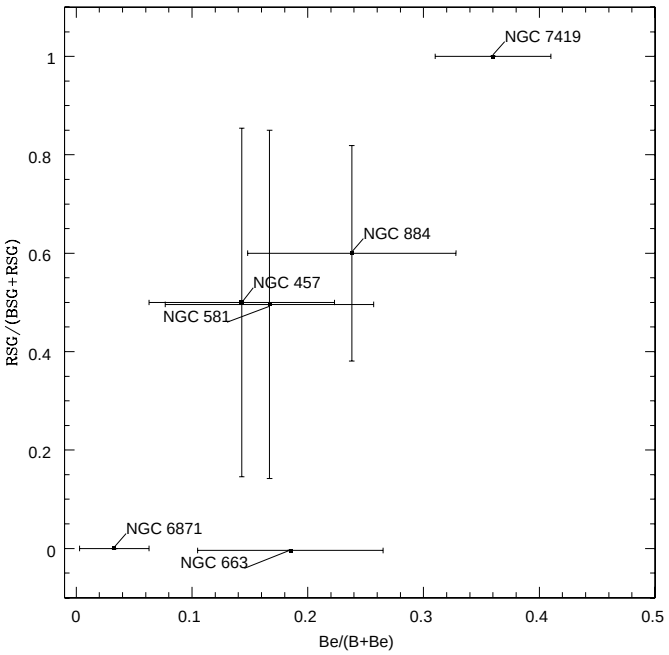

FIG. 12.—Comparison of RSG/(BSG + RSG) with the frequency of Be stars in open clusters that contain at least two supergiants.

However, the metallicity of NGC 7419 is most likely solar, i.e., not low, as this cluster is located in the Galactic disk at a similar Galactocentric distance as the Sun (Eggenberger, Meynet, & Maeder 2002). Unfortunately, we were unable to find in the literature any direct, spectroscopic determinations of the metallicity or rotation of stars in NGC 7419. The fact that NGC 7419 contains a high frequency of Be stars and a low blue-to-red supergiant ratio indicates that rapid rotation of massive stars is also possible at normal metallicity, with the same consequences on the evolution of these stars (see, e.g., Heger & Langer 2000). A possible explanation for this is that the stars in NGC 7419 were formed from a giant molecular cloud with significantly higher internal motions than its average surroundings.

REFERENCES

Aller, L. H. 1963, Astrophysics, the Atmospheres of the Sun and Stars (2d ed.; New York: Ronald Press)
Beauchamp, A., Moffat, A. F. J., & Drissen, L. 1994, ApJS, 93, 187
Cervino, M., & Mas-Hesse, J. M. 1994, A&A, 284, 749
Cowley, A. P., Dawson, P., & Hartwick, F. D. A. 1979, PASP, 91, 628
Eggenberger, P., Meynet, G., & Maeder, A. 2002, A&A, 386, 576
Gray, D. F. 1992, The Observation and Analysis of Stellar Photospheres (Cambridge: Cambridge Univ. Press)
Heger, A., & Langer, N. 2000, ApJ, 544, 1016
Humphreys, R. M., & McElroy, D. B. 1984, ApJ, 284, 565
Keller, S. C., Wood, P. R., & Bessell, M. S. 1999, A&AS, 134, 489
Kurucz, R. 1993, CD-ROM 13, ATLAS9 Stellar Atmosphere Programs and 2km/s Grid (Cambridge: Smithsonian Astro. Obs.)
Langer, N. 1991a, A&A, 252, 669
———. 1991b, A&A, 248, 531
Langer, N., & Maeder, A. 1995, A&A, 295, 685
Maeder, A., Grebel, E. K., & Mermilliod, J.-C. 1999, A&A, 346, 459
Maeder, A., & Meynet, G. 1989, A&A, 210, 155
———. 2000, ARA&A, 38, 143
———. 2001, A&A, 373, 555
Mermilliod, J., & Maeder, A. 1986, A&A, 158, 45
Origlia, L., Goldader, J. D., Leitherer, C., Schaerer, D., & Oliva, E. 1999, ApJ, 514, 96
Pigulski, A., & Kopacki, G. 2000, A&AS, 146, 465
Schild, R., & Romanishin, W. 1976, ApJ, 204, 493
Schulte-Ladbeck, R. E., & Hopp, U. 2001, in Dwarf Galaxies and Their Environment, ed. K. S. De Boer, R.-J. Dettmar, & U. Klein (Aachen: Shaker), 89
Tuchman, Y., & Wheeler, J. C. 1989a, ApJ, 346, 417
———. 1989b, ApJ, 344, 835